condensed matter

MDPI

Article

Sub-THz Waveguide Spectroscopy of Coating Materials for Particle Accelerators

Andrea Passarelli [1,2], Can Koral [2], Maria Rosaria Masullo [2], Wilhelmus Vollenberg [3], Lucia Lain Amador [3] and Antonello Andreone [1,2,*]

1 Physics Department, University of Naples "Federico II", 80131 Naples, Italy; andrea.passarelli@unina.it
2 INFN Naples Unit, 80131 Naples, Italy; ckoral@na.infn.it (C.K.); masullo@na.infn.it (M.R.M.)
3 CERN TE-VSC-SCC, CH-1211 Geneve, Switzerland; Wil.Vollenberg@cern.ch (W.V.); lucia.lain.amador@cern.ch (L.L.A.)
* Correspondence: andreone@unina.it; Tel.: +39-081-2530324

Received: 20 December 2019; Accepted: 15 January 2020; Published: 20 January 2020

Abstract: The electromagnetic characterisation of different materials for the inner wall coating of beam pipes is a long-standing problem in accelerator physics, regardless the purpose they are used for, since their presence may affect in an unpredictable way the beam coupling impedance and therefore the machine performance. Moreover, in particle accelerators and storage rings of new generation very short bunches might be required, extending far in frequency the exploration of the beam spectrum and rendering therefore more and more important to assess the coating material response up to hundreds of GHz. This paper describes a time domain method based on THz waveguide spectroscopy to infer the coating properties at very high frequencies. The technique has been tested on Non Evaporable Getter thick films deposited by DC magnetron sputtering on copper plates.

Keywords: THz; waveguide spectroscopy; coating materials; particle accelerators

1. Introduction

An important step towards the development of a new generation of accelerators and light sources is the special treatment of the vacuum chamber surface, in order to avoid electron cloud (e-cloud) effects that may degrade the machine performance and limit its maximum luminosity.

The e-cloud mechanism starts when the synchrotron radiation, emitted by the beam, creates a large number of photoelectrons at the accelerator wall surface. These primary electrons may cause secondary emission or be elastically reflected [1]. If the value of secondary electron yield (SEY) of the surface material is larger than unity, the number of electrons starts growing exponentially and may lead to beam instabilities and other detrimental side effects [2,3]. It is therefore important to keep the value of SEY as low as possible. Moreover, materials with low photoemission would make not necessary any surface conditioning or in situ heating of the beampipe, which translates in a reduction of machine dead time between experiments.

Reduction of the SEY value in specific sections of the accelerator is therefore mandatory, and an extensive search for the best possible candidates for the pipe internal coating has been extensively carried out in the last years. Amongst other materials, amorphous carbon (a-C) have been thoroughly tested [4] and used [5] at different CERN facilities [6] with very effective results. Another interesting class of materials is non-evaporable getter (NEG) alloys [7], that can be deposited on the inner wall of a vacuum chamber in large accelerators, transforming it from a source of gas into an effective pump. In addition to pumping, NEG films lead to reduced induced gas desorption and secondary electron yields. However, the use of a coating material in an accelerator, being it for the SEY reduction or for the vacuum improvement or both, unavoidably changes the overall surface impedance, possibly producing as adverse effect beam instability because of its electromagnetic interaction with

the surroundings. Therefore, before its insertion in the beam pipe, an accurate electromagnetic characterization is required, for building a reliable impedance model and pinpointing possible problems and performance limitations in modern particle accelerators and storage rings [8].

In the last years, the mitigation properties of coatings have been rarely tested under an electromagnetic field and in the microwave region only [9]. Since beam spectrum may extend up to the very high frequency regime, depending on the bunch length, it might be important to perform an in-depth evaluation of the resistive wall impedance up to millimeter waves and beyond.

Recently, the impedance of NEG films has been measured in frequency domain in the sub-THz range, directly depositing 1–2 μm of the material on the lateral walls of a calibrated waveguide [10,11]. This method can be easily extended to the characterisation of other coating in thin film form, however has its own drawbacks, specifically local in-homogeneity with blistering and peel-off, constraints in sample dimensions, and impossibility to re-use the test system (the waveguide) for further measurements.

An alternative approach is time domain waveguide spectroscopy [12], which has been widely used in the past to obtain high resolution absorption spectra of molecular solids [12], or for the characterisation of thin samples [13,14]. This is done by usually resorting to metallic waveguides since, depending on the design, they can provide a long interaction length and a very high confinement of the electromagnetic field [15], resulting in a significant sensitivity enhancement. Besides that, the use of calibrated devices makes possible the development of characterisation techniques that are both precise and reliable.

With this aim, we have developed a tailored waveguide with integrated pyramidal horn antennas and a removable part where the coating is deposited, which can be placed with ease in the optical path of a THz spectrometer. The design allows us to measure in a simple way large area coating deposited on metallic plates as in the case of accelerators, where averaged quantities are needed. This technique has been successfully used to characterize NEG samples deposited on both sides of thin copper slabs inserted in a circular waveguide [16]. In the case of amorphous carbon however, because of the high temperature growth and the demanding sample thickness requirement, two side deposition is not a feasible approach, because the slab will experience mechanical stress followed by sample peel-off.

Moreover, the transition from the horns to the waveguide, because of the different transverse sections, makes the performance of this device very sensitive to mechanical imperfections and deformations. We designed therefore a modified square waveguide where the transition from antenna to the device is ideally removed, since the horn inner aperture and the waveguide transverse section fully overlap. This results in an increased robustness and a better efficiency of the waveguide in the collection of the THz signal. A major drawback is the reduction by more than 50% in cross section when compared with the circular waveguide, and as a consequence a strong decrease of signal transmitted through the device.

Here we present a detailed description of the high resolution waveguide spectroscopy setup and the analytical method developed for the extraction of the sample electromagnetic properties. In order to validate the technique, we measured the sub-THz response of two coating NEG layers about 4 μm thick deposited using DC magnetron sputtering on both sides of copper plates, and evaluate their conductivity.

2. Materials and Methods

2.1. The Device under Test

Ti-Zr-V NEG coatings are grown at the CERN deposition facilities [4] on both sides of copper plates by using a DC magnetron sputtering technique with Krypton as process gas at a working pressure of 7×10^{-4} mbar (see Figure 1a). An alloyed disc cathode with 33.3% atomic nominal relative composition of Titanium, Zirconium and Vanadium is placed at a distance of 200 mm from the substrate. The applied tension and current are 294 V and 750 mA respectively, for a total power

of 220 W. The complete deposition, giving on average 4 µm thickness, lasts about two days at a growth rate of 1.4 nm/s. During the process, in order to prevent thermal induced deformations the plate is held in an aluminum frame, that in turn is placed on a rotating axis to ensure a homogeneous deposition on both sides of the slab (see Figure 1b). Local composition and thickness of the coating have been checked using X-ray fluorescence (XRF) measurements along the median line of the slab (the waveguide longitudinal axis), showing that samples keep the target composition within 10% and a uniform profile ±2% with an average surface roughness of 0.2 µm [10,17].

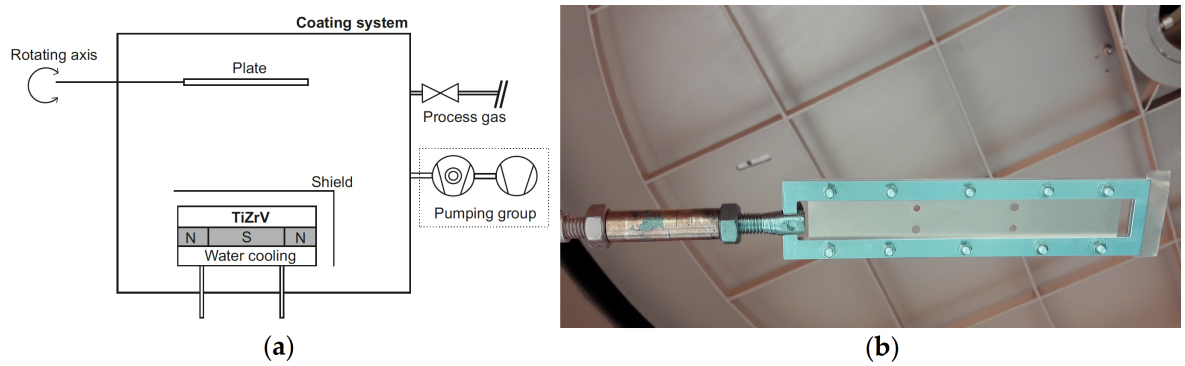

Figure 1. Non-evaporable getter (NEG) deposition setup. (**a**) Drawing of the system; (**b**) detail of the copper slab placed in the aluminum frame. The four holes shown in the picture are used for the alignment in the waveguide during THz measurements.

For the spectroscopy measurements, we use a gold plated brass device (shown in Figure 2) consisting in a parallelepiped of $16 \times 12 \times 140$ mm^3 machined in two identical pieces. A diagonal waveguide is formed by milling a square cross-section channel, rotated by 45° and 62 mm long, in both halves. Two symmetrical pyramidal horn antennas are embedded in both sides of the structure in order to enhance the electromagnetic signal collection and radiation. Moreover, their inner aperture coincides with the waveguide section, ensuring a smooth transition to the waveguide itself without abrupt changes in the device impedance [18]. Disassembling the device, the thin copper slab with the NEG material deposited on both sides can be easily inserted for the sample characterization. The slab has the same length as the device (140 mm) and thickness 0.050 mm.

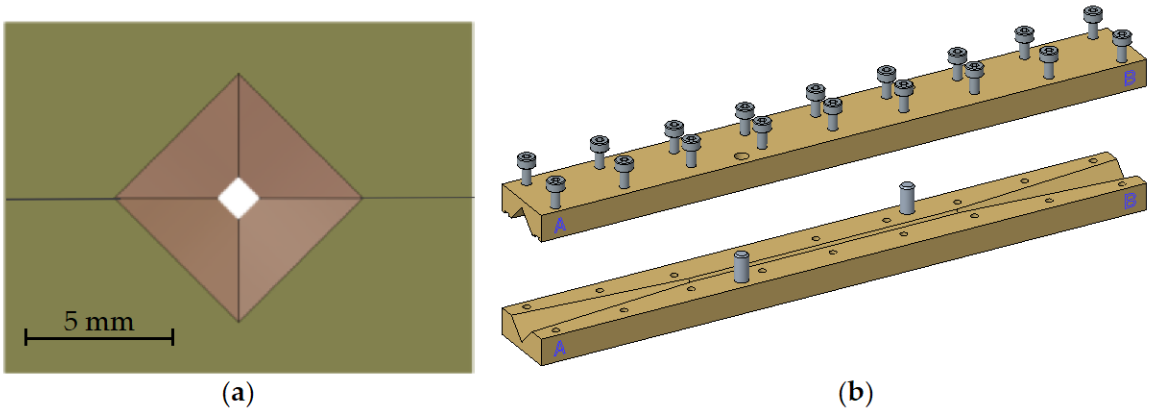

Figure 2. Sketch of the device used for the spectroscopy measurements, consisting in a diagonal section waveguide ending with two pyramidal horn antennas. (**a**) Front view of the assembled device; (**b**) open view of the waveguide and the embedded antennas. The overall size of the device is $16 \times 12 \times 140$ mm^3.

The dimensions and the material used for the waveguide fabrication are reported in Table 1. For the pyramidal horns, maximum and minimum apertures along their length are indicated.

Table 1. Technical specifications of device under test.

Material	**Brass (Au Plated)**
Waveguide	Diagonal
Length [mm]	62
Side [mm]	1.1
Transition	Pyramidal
Length [mm]	39
Side [mm]	$6 \rightarrow 1.1$
Total Length [mm]	140

These dimensions have been chosen in order to have a single mode propagation inside the diagonal waveguide and in the two pyramidal transitions. Due to the central slab inserted along the longitudinal direction, the first mode that can propagate through the structure is the sum of the $TE_{1,0}$ and $TE_{0,1}$. The second allowed mode, given the boundary conditions and the waveguide symmetry, is the sum of $TE_{2,1}$ and $TE_{1,2}$ [19]. For an internal side of the diagonal waveguide of 1.1 mm, the usable frequency window for a single mode propagation ranges from 135 GHz to 300 GHz.

2.2. Sub-THz System

Sub-THz measurements are carried out using a time domain spectrometer (TDS) operating in transmission mode. The setup is based on a commercial THz-TDS system (TERA K15 by Menlo Systems) customized for the waveguide characterization. The system is driven by a femtosecond fiber laser @1560 nm with an optical power <100 mW and a pulse duration <90 fs. Fiber-coupled photoconductive antenna modules are utilized for both electric field signal emission and detection. A fast opto-mechanical line with a maximum scanning range of approximately 300 ps is used to control the time delay between the pump and the probe beam.

TPX (polymethylpentene) lenses are used to collimate the short (1–2 ps) linearly polarized pulse on the waveguide, producing a Gaussian-like beam with a waist of approximately 8 mm in diameter and a quasi-plane wave phase front. This is a standard configuration commonly used to perform transmission measurements on a number of different materials [20]. A sketch of the optical setup is shown in Figure 3.

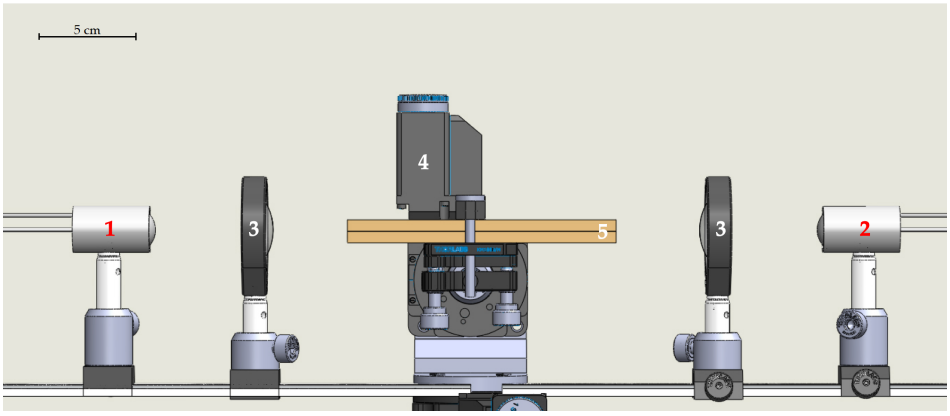

Figure 3. Side view of the opto-mechanical setup utilized for the measurements: (1) emitter, (2) detector, (3) TPX collimating lenses, (4) micrometric alignment system, (5) waveguide with embedded antennas.

For an accurate control of the optical coupling between the free space signal and the input and output horn antennas, the lower part of the waveguide is fixed on a kinematic mount with a micrometric goniometer. Coated slabs are inserted and replaced by removing the upper part only.

The electric field signal as a function of time is recorded for each sample by averaging 1000 pulses for an overall acquisition time of 10 min, in order to minimize the signal-to-noise ratio.

Frequency dependent transmission curves are obtained through the application of a standard FFT algorithm. In the experiment, the frequency resolution is set to about 8 GHz, determined by the scanning range of the delay line.

2.3. The Analytical Method

The conductivity value of the coated material is obtained from the comparison between the signal amplitude transmitted through the waveguide with the coated slab and the one obtained with an uncoated slab used as a reference.

The attenuation both in the diagonal waveguide A_{diag} and in the pyramidal transitions A_{pyr}, considering the propagation of the sum of two modes $TE_{1,0}$ and $TE_{0,1}$, is [21,22]:

$$A_{\text{diag}} = A_{\text{pyr}} = \frac{1}{2} Re(Z_S) \frac{\int |\mathbf{n} \times (\mathbf{H}_{1,0} + \mathbf{H}_{0,1})|^2 \, dl}{Re(Z_{1,0}) \, |I_{1,0}|^2 + Re(Z_{0,1}) \, |I_{0,1}|^2} \tag{1}$$

where $Z_{i,j}$ is the i, j mode impedance and $I_{i,j}$ is the relevant excitation current. The field components used in Equation (1) are:

$$H_{x_{1,0}} = I_{1,0} \frac{\sqrt{2}}{a} \cos\left(\frac{\pi}{a} x\right) \tag{2}$$

$$H_{y_{1,0}} = I_{1,0} \frac{\sqrt{2}}{a} \cos\left(\frac{\pi}{a} y\right), \tag{3}$$

where a is the side of the diagonal waveguide. In case of coating material, the expression of Z_S is:

$$Z_S = Z_{\text{coat}} \frac{Z_{\text{cu}} + j Z_{\text{coat}} \tan(k_{\text{coat}} d)}{Z_{\text{coat}} + j Z_{\text{cu}} \tan(k_{\text{coat}} d)}, \tag{4}$$

where d is the coating thickness. When $d = 0$ there is no coating and $Z_S = Z_{\text{cu}}$. The characteristic impedance in the Leontovich approximation for a metallic case ($\epsilon'' \gg \epsilon'$) is [21]:

$$Z = (1 + j) \sqrt{\frac{\omega \mu}{2\sigma}} = \frac{1 + j}{\sigma \delta} \tag{5}$$

where μ is the total permeability, $\omega = 2\pi f$, and σ the material conductivity.

The propagation constant under the same condition is

$$k = (1 - j) \sqrt{\frac{\sigma \omega \mu}{2}} = \frac{1 - j}{\delta}, \tag{6}$$

where δ is the skin-depth defined as

$$\delta = \sqrt{\frac{2}{\sigma \omega \mu}} \tag{7}$$

The total attenuation on both sides of the slab in the diagonal waveguide is:

$$A_{diag} = \sqrt{2} \frac{Re(Z_S) k_{z_{\text{diag}}}}{a Z_0 k_0} \left[1 + \frac{2k_{t_{\text{diag}}}^2}{k_{z_{\text{diag}}}^2}\right] l_g \tag{8}$$

where l_g is the length of the waveguide, and

$$k_{t_{\text{diag}}} = \frac{\pi}{a}; \quad k_{z_{\text{diag}}} = \sqrt{k_0^2 - k_{t_{\text{diag}}}^2}$$

We evaluate the relative attenuation in the diagonal waveguide as:

$$RA_{\text{diag}} = A^{\text{coat}}_{\text{diag}} - A^{\text{cu}}_{\text{diag}}. \tag{9}$$

Differently from the contribution in the diagonal section, the attenuation on the slab given by the symmetric input and output transitions is not constant, since the antenna aperture changes along the horn length. The total attenuation in the single pyramidal transition is:

$$\begin{aligned} A_{\text{pyr}} &= \int_0^{l_t} \sqrt{2}\frac{Re(Z_S)k_{z_{\text{pyr}}}(z)}{c(z)Z_0k_0}\left[1+\frac{2k^2_{t_{\text{pyr}}}(z)}{k^2_{z_{\text{pyr}}}(z)}\right]dz \\ &= \frac{1}{\sqrt{2}}\frac{Re(Z_s)}{Z_0}\left\{-\frac{1}{2b_1}\log\left[\frac{\sqrt{1-\left(\frac{\pi}{k_0B}\right)^2}-1}{\sqrt{1-\left(\frac{\pi}{k_0B}\right)^2}+1}\frac{\sqrt{1-\left(\frac{\pi}{k_0b}\right)^2}+1}{\sqrt{1-\left(\frac{\pi}{k_0b}\right)^2}-1}\right]\right. \\ &\left.+\frac{2}{b_1}\left[\sqrt{\left(\frac{\pi}{k_0B}\right)^2}-\sqrt{\left(\frac{\pi}{k_0b}\right)^2}\right]\right\} \end{aligned} \tag{10}$$

where

$$k_{t_{\text{pyr}}}(z) = \frac{\pi}{c(z)}; \quad k_{z_{\text{pyr}}}(z) = \sqrt{k_0^2 - k^2_{t_{\text{pyr}}}(z)}$$

and

$$c(z) = b + zb_1 = b + z\frac{B-b}{l_t}$$

expresses how the side of the horn changes along the transition. l_t is the longitudinal length of the transition, B and b are the side dimension at the entrance and exit of the pyramidal horn transition respectively. Since the transitions are connected to the diagonal waveguide, then $b = a$.

The relative attenuation in the pyramidal transition is:

$$RA_{\text{pyr}} = A^{\text{coat}}_{\text{pyr}} - A^{\text{cu}}_{\text{pyr}}. \tag{11}$$

The total relative attenuation is given by the formula:

$$RA_{\text{Total}} = RA_{\text{diag}} + 2\,RA_{\text{pyr}}, \tag{12}$$

resorting to Equations (9) and (11).

3. Results and Discussion

The electromagnetic characterization of the NEG coatings in the sub-THz region is realized performing time domain (TD) measurements of the electromagnetic wave propagating inside the specifically designed waveguide with a thin central copper slab, where the material under test is deposited on both sides. The THz beam is polarized with its electric field parallel to the waveguide slab. The use of a device having a square cross section marks an improvement in terms of beam collection efficiency with respect to previous measurements [16]. However, compared to the free space signal, the transmitted electric field is in the order of 10% only. Figure 4 shows the difference in the signal transmitted in air and in the squared waveguide, without and with slab.

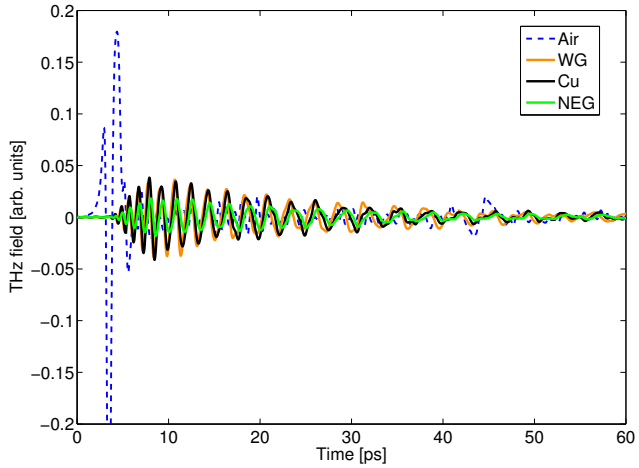

Figure 4. THz time domain averaged signal propagating in air (dashed line), through the waveguide without (orange, continuous line) and with copper (black, continuous line) or NEG coated (green, continuous line) slab.

The TD curves show that the presence of the NEG layer clearly introduces not only a strong attenuation of the signal but also a significant dispersion. When the THz signal passes through the device, the ps-scale input pulse with respect to the case of free space transmission is strongly reshaped by the reflections inside the waveguide and broadened to more than 50 ps. The stretching of the transmitted signal, compared with the free space input pulse, is due to the strongly dispersive character of the waveguide, that acts as a delay line [23]. After the main burst, at around 120 ps interference features (not shown) appear, due to round-trip reflections inside the waveguide, that have been removed in the subsequent frequency analysis.

In frequency domain, the amplitude spectra are obtained using FFT (Fast Fourier Transform) analysis and are presented in Figure 5 for both samples in comparison with the bare copper slab, with the waveguide without the slab, and with air only.

Data are shown up to the frequency where single mode propagation in the waveguide holds. This ensures that there is no interference from higher order modes, which can produce a modification of the field distribution, as discussed in detail in Section 2.3. The cut-off frequency of the first mode propagating inside the waveguide (approximately 150 GHz) can be clearly seen.

In the graph, the NEG coated samples (red and green dots) behave in a similar way, with a marked difference in amplitude (between 4 and 6 dB on average) with respect to copper (black dots) and slightly increasing at higher frequencies. Changing the design of the waveguide from circular to square therefore does imply a better sensitivity to the coating material properties, since the weight of the slab losses relatively to the overall waveguide losses increases, but this is done at the expense of a reduction in the amplitude of the collected signal, raising noise and data fluctuations.

From the comparison with the uncoated slab, the (relative) attenuation given by the losses produced in the device through its overall length (horn antennas and waveguide) by the coating material can be evaluated.

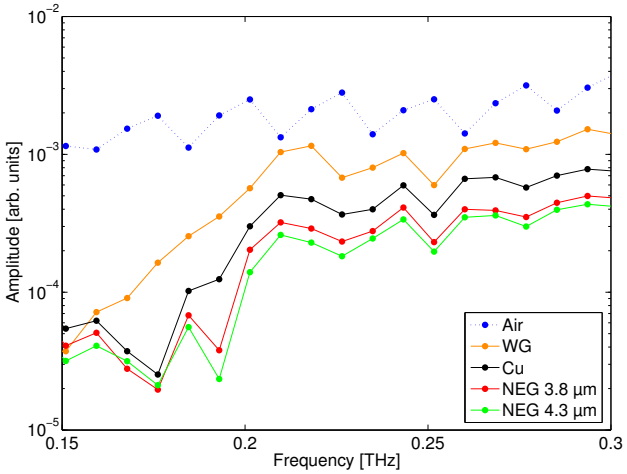

Figure 5. Frequency spectrum showing the averaged amplitude transmission data in air (dashed line-to-point curve), through the waveguide without (orange line-to-point curve) and with copper (black line-to-point curve) or 3.8 μm and 4.3 μm NEG coated (red and green line-to-point curves respectively) slabs.

In Figure 6, the measured relative attenuation due to both the 3.8 μm and 4.3 μm NEG coatings with respect to the copper reference are shown (red and green dots respectively). Data below 200 GHz have been discarded to avoid artifacts in the spectrum due to group and phase velocity dispersion, especially pronounced near the cut off frequency. Therefore, results are presented in the range 200–300 GHz.

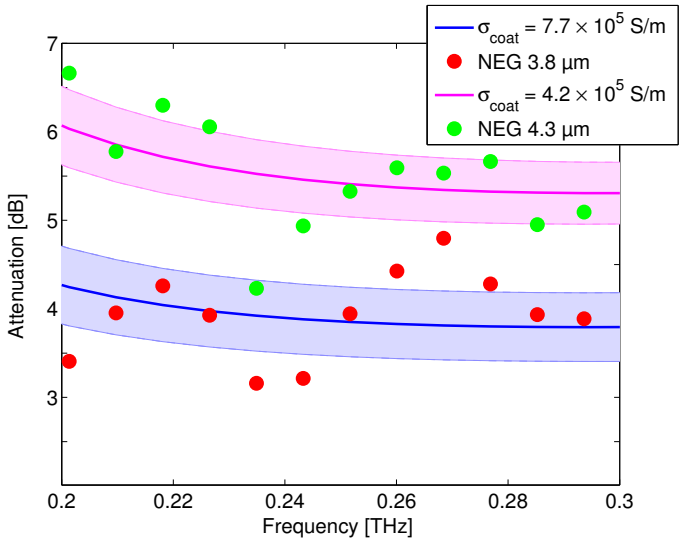

Figure 6. Experimental relative attenuation as a function of frequency on the NEG coated slab of 3.8 μm and 4.3 μm (red and green dots respectively) and best fit curves (blue and magenta lines respectively).

The conductivity value σ_{coat} of the coating material is obtained resorting on the analytical tool detailed in Section 2.3. From the best fit of the analytical formula, we yield $\sigma_{\text{coat}} = (7.7 \pm 1.1) \times 10^5$ S/m for the 3.8 μm sample, and $\sigma_{\text{coat}} = (4.2 \pm 0.5) \times 10^5$ S/m for the 4.3 μm sample. Magenta and blue continuous lines in Figure 6 show the analytically evaluated attenuation for the two estimated conductivities, taken from Equation (12) in Section 2. For both curves the 95% confidence interval on the attenuation due to the conductivity evaluation uncertainties is also displayed as shaded area. The difference observed between the two samples might be an indication of an increased disorder,

that translates in poorer transport properties and therefore lower conductivity, caused by the larger thickness.

Resorting on [24], we can also evaluate the effect of sample roughness on the NEG conductivity. Using the average roughness value for our samples (0.2 μm), we estimate a maximum conductivity reduction of the order of 8%, that lies within the measurement error band in our frequency range.

Results agree fairly well both with previous data obtained on different NEG samples using the circular waveguide [16] and DC (direct current) conductivity values extracted using the frequency domain approach [10]. Nevertheless, differently to these latter measurements, a TD method allows to evaluate the electromagnetic properties of coatings in a reliable and simple way exploiting tailored (and reusable) waveguides. The knowledge of σ_{coat} under operating conditions (coating deposited on a metallic slab) is extremely useful for the evaluation of the real part of the surface impedance as a function of frequency, that is currently used for modeling the resistive wall component of the beam impedance in modern accelerators.

Author Contributions: A.P. and A.A. conceived the experiment. A.P., M.R.M. and A.A. developed the theory for the electromagnetic characterization of coating material in a waveguide. A.P. and C.K. performed the THz measurements. W.V. and L.L.A. realized the NEG samples. A.P. ad A.A. wrote the manuscript, with contributions from all authors. A.A. supervised the activity. All authors have read and agreed to the published version of the manuscript.

Funding: This research has been funded by the CLIC project in the framework of the CERN-INFN Naples collaboration (KN4542/BE Addendum no.13 to Agreement KN3083). Partial support from INFN Projects "TERA" and "MICA" is gratefully acknowledged.

Acknowledgments: The authors thank S. Calatroni, P. Costa Pinto, R. Corsini, Y. Papaphilippou, and M. Taborelli from CERN for their support.

Conflicts of Interest: The authors declare no conflict of interest.

References

1. Furman, M.A. Electron Cloud Effects in Accelerators. *arXiv* **2013**, arXiv:1310.1706.
2. Rumolo, G.; Ruggiero, F.; Zimmermann, F. Simulation of the electron-cloud build up and its consequences on heat load, beam stability, and diagnostics. *Phys. Rev. Spec. Top.-Accel. Beams* **2001**, *4*, 012801.10.1103/PhysRevSTAB.4.012801. [CrossRef]
3. Cimino, R.; Gonzalez, L.A.; Larciprete, R.; Di Gaspare, A.; Iadarola, G.; Rumolo, G. Detailed investigation of the low energy secondary electron yield of technical Cu and its relevance for the LHC. *Phys. Rev. Spec. Top.-Accel. Beams* **2015**, *18*, 051002.10.1103/PhysRevSTAB.18.051002. [CrossRef]
4. Yin Vallgren, C.; Arduini, G.; Bauche, J.; Calatroni, S.; Chiggiato, P.; Cornelis, K.; Pinto, P.C.; Henrist, B.; Métral, E.; Neupert, H.; et al. Amorphous carbon coatings for the mitigation of electron cloud in the CERN Super Proton Synchrotron. *Phys. Rev. Spec. Top.-Accel. Beams* **2011**, *14*, 071001.10.1103/PhysRevSTAB.14.071001. [CrossRef]
5. Taborelli, M.; Chiggiato, P.; Costa Pinto, P.; Cruikshank, P. *Nine Years of Carbon Coating Development for the SPS Upgrade: Achievements and Heritage*; Technical Report CERN-ACC-2016-0010; CERN: Geneva, Switzerland, 2015.
6. Palmer, M.; Livezey, J.; Wolski, A.; Zwaska, R.; Sagan, D.; Savino, J.; Williams, H.; Antoniou, F.; Tan, C.Y.; Sikora, J. Electron Cloud at Low Emittance in CesrTA. In Proceedings of the International Particle Accelerator Conference, Kyoto, Japan, 23–28 May 2010.
7. Benvenuti, C.; Chiggiato, P.; Pinto, P.C.; Santana, A.E.; Hedley, T.; Mongelluzzo, A.; Ruzinov, V.; Wevers, I. Vacuum properties of TiZrV non-evaporable getter films. *Vacuum* **2001**, *60*, 57–65. [CrossRef]
8. Migliorati, M.; Belli, E.; Zobov, M. Impact of the resistive wall impedance on beam dynamics in the Future Circular e^+e^- Collider. *Phys. Rev. Accel. Beams* **2018**, *21*, 041001.10.1103/PhysRevAccelBeams.21.041001. [CrossRef]
9. Federmann, S.; Caspers, F.; Mahner, E. Measurements of electron cloud density in the CERN Super Proton Synchrotron with the microwave transmission method. *Phys. Rev. Spec. Top.-Accel. Beams* **2011**, *14*, 012802.10.1103/PhysRevSTAB.14.012802. [CrossRef]

10. Koukovini-Platia, E.; Rumolo, G.; Zannini, C. Electromagnetic characterization of nonevaporable getter properties between 220–330 and 500–750 GHz for the Compact Linear Collider damping rings. *Phys. Rev. Accel. Beams* **2017**, *20*, 011002.10.1103/PhysRevAccelBeams.20.011002. [CrossRef]
11. Koukovini Platia, E. High Frequency Effects of Impedances and Coatings in the CLIC Damping Rings. Ph.D. Thesis, Ecole Polytechnique, Lausanne, Switzerland, 2015.
12. Theuer, M.; Melinger, J.S. High Resolution Waveguide Terahertz Time-Domain Spectroscopy. *J. Infrared Millim. Terahertz Waves* **2011**, *32*, 1267–1284.10.1007/s10762-011-9816-3. [CrossRef]
13. Razanoelina, M.; Kinjo, R.; Takayama, K.; Kawayama, I.; Murakami, H.; Mittleman, D.M.; Tonouchi, M. Parallel-Plate Waveguide Terahertz Time Domain Spectroscopy for Ultrathin Conductive Films. *J. Infrared, Millim. Terahertz Waves* **2015**, *36*, 1182–1194.10.1007/s10762-015-0194-0. [CrossRef]
14. Khachatrian, A.; Melinger, J.S.; Qadri, S.B. Waveguide terahertz time-domain spectroscopy of ammonium nitrate polycrystalline films. *J. Appl. Phys.* **2012**, *111*, 093103. [CrossRef]
15. Zhang, J.; Grischkowsky, D. Adiabatic compression of parallel-plate metal waveguides for sensitivity enhancement of waveguide THz time-domain spectroscopy. *Appl. Phys. Lett.* **2005**, *86*, 061109.10.1063/1.1863439. [CrossRef]
16. Passarelli, A.; Bartosik, H.; Rumolo, G.; Vaccaro, V.G.; Masullo, M.R.; Koral, C.; Papari, G.P.; Andreone, A.; Boine-Frankenheim, O. Novel measurement technique for the electromagnetic characterization of coating materials in the sub-THz frequency range. *Phys. Rev. Accel. Beams* **2018**, *21*, 103101.10.1103/PhysRevAccelBeams.21.103101. [CrossRef]
17. Prodromides, A.E.; Levy, F. Non-Evaporable Getter Thin Film Coatings for Vacuum Applications. Ph.D. Thesis, Ecole Polytechnique, Lausanne, Switzerland, 1 September 2002; pp. 95–96.
18. Johansson, J.F.; Whyborn, N.D. The diagonal horn as a sub-millimeter wave antenna. *IEEE Trans. Microw. Theory Tech.* **1992**, *40*, 795–800.10.1109/22.137380. [CrossRef]
19. Lee, C.S.; Lee, S.W.; Chuang, S.L. Plot of Modal Field Distribution in Rectangular and Circular Waveguides. *IEEE Trans. Microw. Theory Tech.* **1985**, *33*, 271–274.10.1109/TMTT.1985.1132998. [CrossRef]
20. Papari, G.P.; Silvestri, B.; Vitiello, G.; De Stefano, L.; Rea, I.; Luciani, G.; Aronne, A.; Andreone, A. Morphological, Structural, and Charge Transfer Properties of F-Doped ZnO: A Spectroscopic Investigation. *J. Phys. Chem. C* **2017**, *121*, 16012–16020.10.1021/acs.jpcc.7b04821. [CrossRef]
21. Marcuvitz, N. *Waveguide Handbook*; IEE: London, UK, 1986.
22. Franceschetti, G. *Electromagnetics: Theory, Techniques, and Engineering Paradigms*; Springer: New York, NY, USA, 1997.
23. Mendis, R.; Mittleman, D.M. Comparison of the lowest-order transverse-electric (TE1) and transverse-magnetic (TEM) modes of the parallel-plate waveguide for terahertz pulse applications. *Opt. Express* **2009**, *17*, 14839–14850.10.1364/OE.17.014839. [CrossRef] [PubMed]
24. Hammerstad, E.; Jensen, O. Accurate Models for Microstrip Computer-Aided Design. In Proceedings of the 1980 IEEE MTT-S International Microwave symposium Digest, Washington, DC, USA, 28–30 May 1980; pp. 407–409.10.1109/MWSYM.1980.1124303. [CrossRef]